PCCP

Physical Chemistry Chemical Physics

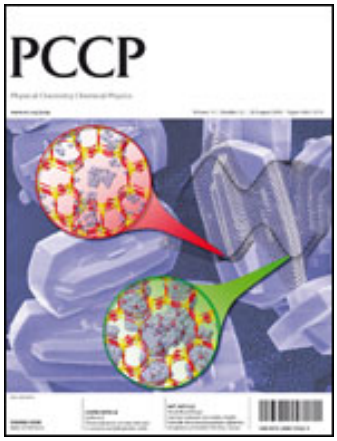

This paper is published as part of a PCCP Themed Issue on:

Water at interfaces

Guest Editor: Martin McCoustra

Editorial

Communications

Papers

Raman spectra of complexes of HNO_3 and NO_3^- with NO_2 at surfaces and with N_2O_4 in solution
Michael A. Kamboures, Wytze van der Veer, R. Benny Gerber and Leon F. Phillips, *Phys. Chem. Chem. Phys.*, 2008, **10**, 4748
DOI: 10.1039/b810081k

Molecular level structure of the liquid/liquid interface. Molecular dynamics simulation and ITIM analysis of the water-CCl_4 system
Lívia B. Pártay, George Horvai and Pál Jedlovszky, *Phys. Chem. Chem. Phys.*, 2008, **10**, 4754
DOI: 10.1039/b807299j

Solvent structures of mixed water/acetonitrile mixtures at chromatographic interfaces from computer simulations
Jörg Braun, Antony Fouqueau, Raymond J. Bemish and Markus Meuwly, *Phys. Chem. Chem. Phys.*, 2008, **10**, 4765
DOI: 10.1039/b807492e

Ion spatial distributions at the liquid–vapor interface of aqueous potassium fluoride solutions
Matthew A. Brown, Raffaella D'Auria, I.-F. William Kuo, Maria J. Krisch, David E. Starr, Hendrik Bluhm, Douglas J. Tobias and John C. Hemminger, *Phys. Chem. Chem. Phys.*, 2008, **10**, 4778
DOI: 10.1039/b807041e

Trapping proton transfer intermediates in the disordered hydrogen-bonded network of cryogenic hydrofluoric acid solutions
Patrick Ayotte, Sylvain Plessis and Patrick Marchand, *Phys. Chem. Chem. Phys.*, 2008, **10**, 4785
DOI: 10.1039/b806654j

Aqueous divalent metal–nitrate interactions: hydration *versus* ion pairing
Man Xu, James P. Larentzos, Mazen Roshdy, Louise J. Criscenti and Heather C. Allen, *Phys. Chem. Chem. Phys.*, 2008, **10**, 4793
DOI: 10.1039/b807090n

Structure and dynamics of water at a clay surface from molecular dynamics simulation
Virginie Marry, Benjamin Rotenberg and Pierre Turq, *Phys. Chem. Chem. Phys.*, 2008, **10**, 4802
DOI: 10.1039/b807288d

Proton mobility in thin ice films: a revisit
Eui-Seong Moon, Chang-Woo Lee and Heon Kang, *Phys. Chem. Chem. Phys.*, 2008, **10**, 4814
DOI: 10.1039/b807730b

Thermodynamics of water intrusion in nanoporous hydrophobic solids
Fabien Cailliez, Mickael Trzpit, Michel Soulard, Isabelle Demachy, Anne Boutin, Joël Patarin and Alain H. Fuchs, *Phys. Chem. Chem. Phys.*, 2008, **10**, 4817
DOI: 10.1039/b807471b

Gas phase hydration of organic ions
Paul O. Momoh and M. Samy El-Shall, *Phys. Chem. Chem. Phys.*, 2008, **10**, 4827
DOI: 10.1039/b809440n

Water photodissociation in free ice nanoparticles at 243 nm and 193 nm
Viktoriya Poterya, Michal Fárník, Milan Ončák and Petr Slavíček, *Phys. Chem. Chem. Phys.*, 2008, **10**, 4835
DOI: 10.1039/b806865h

Electroacoustic and ultrasonic attenuation measurements of droplet size and ζ-potential of alkane-in-water emulsions: effects of oil solubility and composition
Alex M. Djerdjev and James K. Beattie, *Phys. Chem. Chem. Phys.*, 2008, **10**, 4843
DOI: 10.1039/b807623e

Gas hydrate nucleation and cage formation at a water/methane interface
Robert W. Hawtin, David Quigley and P. Mark Rodger, *Phys. Chem. Chem. Phys.*, 2008, **10**, 4853
DOI: 10.1039/b807455k

Hydration water rotational motion as a source of configurational entropy driving protein dynamics. Crossovers at 150 and 220 K
J.-M. Zanotti, G. Gibrat and M.-C. Bellissent-Funel, *Phys. Chem. Chem. Phys.*, 2008, **10**, 4865
DOI: 10.1039/b808217k

Influence of wettability and surface charge on the interaction between an aqueous electrolyte solution and a solid surface
Svetlana Guriyanova and Elmar Bonaccurso, *Phys. Chem. Chem. Phys.*, 2008, **10**, 4871
DOI: 10.1039/b806236f

Molecular dynamics study of hydrated imogolite 2. Structure and dynamics of confined water
Benoît Creton, Daniel Bougeard, Konstantin S. Smirnov, Jean Guilment and Olivier Poncelet, *Phys. Chem. Chem. Phys.*, 2008, **10**, 4879
DOI: 10.1039/b803479f

Assessing the performance of implicit solvation models at a nucleic acid surface
Feng Dong, Jason A. Wagoner and Nathan A. Baker, *Phys. Chem. Chem. Phys.*, 2008, **10**, 4889
DOI: 10.1039/b807384h

Aqueous peptides as experimental models for hydration water dynamics near protein surfaces
Cecile Malardier-Jugroot, Margaret E. Johnson, Rajesh K. Murarka and Teresa Head-Gordon, *Phys. Chem. Chem. Phys.*, 2008, **10**, 4903
DOI: 10.1039/b806995f

Melting behavior of water in cylindrical pores: carbon nanotubes and silica glasses
M. Sliwinska-Bartkowiak, M. Jazdzewska, L. L. Huang and K. E. Gubbins, *Phys. Chem. Chem. Phys.*, 2008, **10**, 4909
DOI: 10.1039/b808246d

Increased interfacial thickness of the NaF, NaCl and NaBr salt aqueous solutions probed with non-resonant surface second harmonic generation (SHG)
Hong-tao Bian, Ran-ran Feng, Yan-yan Xu, Yuan Guo and Hong-fei Wang, *Phys. Chem. Chem. Phys.*, 2008, **10**, 4920
DOI: 10.1039/b806362a

Determination of the electron's solvation site on D_2O/Cu(111) using Xe overlayers and femtosecond photoelectron spectroscopy
Michael Meyer, Julia Stähler, Daniela O. Kusmierek, Martin Wolf and Uwe Bovensiepen, *Phys. Chem. Chem. Phys.*, 2008, **10**, 4932
DOI: 10.1039/b807314g

Breakdown of hydration repulsion between charged surfaces in aqueous Cs^+ solutions
Ronit Goldberg, Liraz Chai, Susan Perkin, Nir Kampf and Jacob Klein, *Phys. Chem. Chem. Phys.*, 2008, **10**, 4939
DOI: 10.1039/b807459n

A macroscopic water structure based model for describing charging phenomena at inert hydrophobic surfaces in aqueous electrolyte solutions
Johannes Lützenkirchen, Tajana Preočanin and Nikola Kallay, *Phys. Chem. Chem. Phys.*, 2008, **10**, 4946
DOI: 10.1039/b807395c

Thermally induced mixing of water dominated interstellar ices
Daren J. Burke, Angela J. Wolff, John L. Edridge and Wendy A. Brown, *Phys. Chem. Chem. Phys.*, 2008, **10**, 4956
DOI: 10.1039/b807220e

Water hydrogen bond analysis on hydrophilic and hydrophobic biomolecule sites
Daniela Russo, Jacques Ollivier and José Teixeira, *Phys. Chem. Chem. Phys.*, 2008, **10**, 4968
DOI: 10.1039/b807551b

Hydronium and hydroxide at the interface between water and hydrophobic media
Robert Vácha, Dominik Horinek, Max L. Berkowitz and Pavel Jungwirth, *Phys. Chem. Chem. Phys.*, 2008, **10**, 4975
DOI: 10.1039/b806432f

Average molecular orientations in the adsorbed water layers on silicon oxide in ambient conditions
Anna L. Barnette, David B. Asay and Seong H. Kim, *Phys. Chem. Chem. Phys.*, 2008, **10**, 4981
DOI: 10.1039/b810309g

Interfacial water structure at polymer gel/quartz interfaces investigated by sum frequency generation spectroscopy
Hidenori Noguchi, Minowa Hiroshi, Taiki Tominaga, Jian Ping Gong, Yoshihito Osada and Kohei Uosaki, *Phys. Chem. Chem. Phys.*, 2008, **10**, 4987
DOI: 10.1039/b807297n

Co-adsorption of water and hydrogen on Ni(111)
Junjun Shan, Jacques F. M. Aarts, Aart W. Kleyn and Ludo B. F. Juurlink, *Phys. Chem. Chem. Phys.*, 2008, **10**, 4994
DOI: 10.1039/b808219g

Water–methanol mixtures: topology of hydrogen bonded network
Imre Bakó, Tünde Megyes, Szabolcs Bálint, Tamás Grósz and Viorel Chihaia, *Phys. Chem. Chem. Phys.*, 2008, **10**, 5004
DOI: 10.1039/b808326f

Determination of the electron's solvation site on D_2O/Cu(111) using Xe overlayers and femtosecond photoelectron spectroscopy

Michael Meyer, Julia Stähler, Daniela O. Kusmierek, Martin Wolf and Uwe Bovensiepen

Received 30th April 2008, Accepted 12th June 2008
First published as an Advance Article on the web 4th July 2008
DOI: 10.1039/b807314g

We investigate the binding site of solvated electrons in amorphous D_2O clusters and D_2O wetting layers adsorbed on Cu(111) by means of two-photon photoelectron (2PPE) spectroscopy. On the basis of different interactions of bulk- or surface-bound solvated electrons with rare gas atoms, titration experiments using Xe overlayers reveal the location of the electron solvation sites. In the case of flat clusters with a height of 2–4 bilayers adsorbed on Cu(111), solvated electrons are found to reside at the ice–vacuum interface, whereas a bulk character is found for solvated electrons in wetting layers. Furthermore, time-resolved experiments are performed to determine the origin of the transition between these different solvation sites with increasing D_2O coverage. We employ an empirical model calculation to analyse the rate of electron transfer back to the substrate and the energetic stabilization of the solvated electrons, which allows further insight into the binding site for clusters. We find that the solvated electrons reside at the edges of the clusters. Therefore, we attribute the transition from surface- to bulk-solvation to the coalescence of the clusters to a closed ice film occurring at a nominal coverage of 2–3 BL, while the distance of the binding sites to the metal–ice interface is maintained.

1. Introduction

The hydrated electron is an excess electron in water that is stabilized in a cavity of surrounding molecules. Since its discovery[1] it has attracted interest in many fields of condensed matter research, as its properties are of great importance in numerous biological, chemical, and physical processes.[2–4] Although the interaction of excess electrons with surrounding water molecules has been investigated extensively in the case of water cluster anions,[5–9] the binding site of the excess charge in such finite systems is still the subject of a long-standing controversy. Theory predicts a transition from surface-bound electrons to an internal binding site with increasing cluster size, *i.e.* increasing number of molecules n, but this transition has not yet been observed experimentally for the predicted cluster sizes. While photoelectron spectroscopy experiments found solvated electrons which were attributed to bulk-bound electrons for clusters[5,10] down to $n = 11$, theory[11] predicts internally bound electrons for clusters with $n \geq 64$. The experimental observation of this transition is also hindered as the photoelectron spectra of water anion clusters depend critically on the preparation conditions. For different backing pressures Verlet *et al.* observed up to three different isomers,[12] and it is *a priori* unclear which isomer corresponds to the respective surface and internal states. Early theoretical studies by Barnett *et al.* investigated the temporal evolution of electron solvation in large ($n = 500$) water and ammonia clusters showing a weakly bound surface state right after attachment of the electron leading to the formation of an internal solvation state.[13] Although experiment[12] and theory[14] recently accessed larger clusters with n up to 200, no quantitative agreement has been achieved so far. The use of rare gas environments in spectroscopic studies of water anion clusters has been suggested to investigate the actual excess electron binding site.[7,15]

Another approach to address fundamental questions of electron solvation dynamics in polar environments is based on surface science techniques.[16,17] Thereby various ice structures can be grown on a single crystal substrate and the properties of photoexcited excess electrons can be studied in a controlled way. For example, by adjusting the temperature of the substrate, amorphous ice structures are grown on a metal surface and information about their morphology can be achieved by means of low-temperature scanning tunnelling microscopy (LT-STM). The dynamics of photoinjected electrons is directly monitored by femtosecond time- and angle-resolved two-photon photoelectron spectroscopy. The transient binding energy of the electrons and additionally its degree of localization can thus be probed without interference with the photohole, which is completely screened by the electrons of the metal substrate. Actually, the respective electron solvation dynamics have been studied for a variety of different polar molecular layers (*e.g.* D_2O, NH_3, alcohols, nitriles) adsorbed on various substrates.[18–21] These electrons typically reside for picoseconds in the amorphous adlayer due to the screening of their charge from the metal states by the polar environment through molecular rearrangement. However, for directionally-bound water molecules on TiO_2, the more rigid bounding inhibits such a screening leading to lifetimes of only a few

Freie Universität Berlin, Fachbereich Physik, Arnimallee 14, 14195 Berlin, Germany

femtoseconds.[22] Solvated electrons have a high capability to induce chemical reactions with coadsorbed molecules such as chlorofluorocarbons (CFC).[3,4,23,24] For instance, Lu and Madey found an enhanced electron-induced dissociation of CFC when coadsorbed with water; the authors attribute this effect to a reaction of the CFC with solvated electrons.[3] The efficiency of such reactions can be enhanced when (i) the lifetime of the solvated electrons is long or (ii) the electron density resides at the molecule–vacuum interface.[24] Thus, information on the electrons' binding site is of fundamental interest. It can be determined by different approaches. Nordlund *et al.* measured ultrafast delocalization rates of core excited electrons in liquid water as well as in crystalline ice films employing core–hole decay spectroscopy.[25] They found broken or weak hydrogen bonds at the surface of the ice, providing states for the initial electron localization.

To address the question of the solvation site we coadsorb a dielectric medium, *i.e.* xenon atoms, onto the water ice to influence the electrostatic environment of the excess electrons. Related experiments have been performed to study the effect of rare gas films on the ultrafast electron dynamics of image-potential states on metal surfaces.[26–28] As shown for amorphous water ice clusters adsorbed on Cu(111), the spectral signature of the solvated electrons is modified by titration of surface binding sites with xenon atoms.[29]

In the framework of the present article we focus on the electron solvation site in amorphous ice layers and a more detailed determination of the binding site of surface-solvated electrons in ice clusters. We extend earlier studies, where we have shown that excess electrons can be stabilized transiently in amorphous ice layers adsorbed on metal substrates.[20,30] As these electrons, which are photoinjected into the ice layer, are stabilized by the formation of a transient solvated electron–water complex, we refer in the following to these transient species as solvated electrons for simplicity. Due to the finite interaction of such solvated electrons with the metal substrate, they present a short residence time of $\sim$1 ps before they decay back to the metal.

The studies have been performed on ice clusters and closed multilayers prepared on a monocrystalline Cu(111) metal substrate. On other metal substrates like Pt(111) and Pd(111) such a comparison between clusters and layers is not possible, as amorphous ice wets the substrate and grows approximately layer by layer.[31] In our experiment, the ability to distinguish between surface- and bulk-bound electrons is obtained by adsorbing a xenon adlayer on top of the adsorbed ice clusters or layers. Under ultrahigh vacuum conditions accommodation of the xenon atoms inside the water film can be ruled out.[32] The basic principle of the 2PPE with xenon titration is depicted in Fig. 1. Electrons in the copper substrate below the Fermi level are excited by an ultraviolet (UV) pump pulse, with a photon energy $h\nu_1$, into intermediate bound states where they can be transferred into the conduction band of the ice. Then, the electrons localize and solvate in binding sites where they are probed by a second visible (VIS) probe pulse $h\nu_2$. Depending on whether the solvated electrons reside in the bulk of the ice or at the ice/xenon interface, the Xe atoms will influence the electronic properties of the electrons, such as their binding energy or their lifetime. In the case of bulk solvation, no significant change of the photoelectron spectra is expected (Fig. 1a). Only the net electric field of the electron-solvation shell complex could polarize the xenon, which would yield minor changes in the 2PPE spectrum. If the electron is located at the surface of the ice layer, the electron wave function will be modified due to the direct polarization of the rare gas atoms and, for example, a change of the binding energy of the solvated electron is expected (ΔE, Fig. 1b). We complement the 2PPE-spectroscopy work by femtosecond time-resolved 2PPE to analyse the ultrafast electron transfer of solvated electrons in these structures as it is sensitive to the coupling of the electrons with the metal substrate. In combination with empirical model calculations, this allows us to distinguish whether the electrons reside on the top or at the edges of the ice clusters.

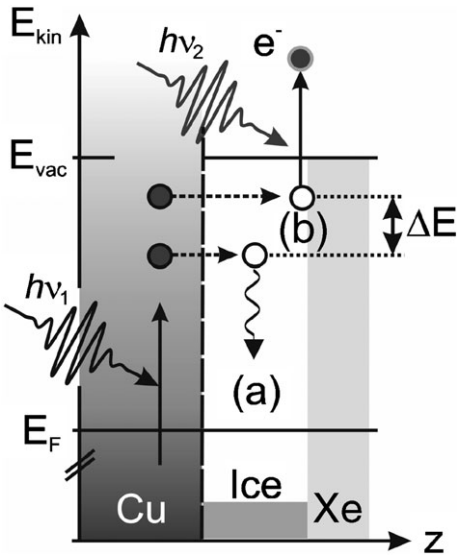

Fig. 1 Scheme of the Xe overlayer experiment and 2PPE. Due to the different interaction of (a) bulk- and (b) surface-bound electrons with the coadsorbed xenon, which may result in a change in the electron's binding energy ΔE, different solvation sites can be distinguished.

2. Experimental methods and sample characterization

The experiments were performed in an ultrahigh vacuum (UHV) chamber with a base pressure below 10^{-10} mbar. Amorphous ice clusters and wetting ice layers are grown by expansion of D_2O vapour through a 50 μm diameter pinhole into UHV onto a Cu(111) surface kept at 85 K. D_2O was chosen as it allows for a distinct separation of the desorption from the D_2O ice adlayer from a residual background of H_2O in thermal desorption spectroscopy. Furthermore, by changing D_2O to H_2O no isotope effect of the stabilization rate has been observed in earlier studies.[30] Before water adsorption, the Cu(111) sample is prepared by cycles of Ar^+ sputtering and annealing as described in ref. 33. For coverages Θ below 2 bilayers (BL),[20] the adsorbed water forms clusters on the surface. With increasing Θ, a transition to wetting layers is observed by means of low-temperature scanning tunnelling microscopy (LT-STM) and 2PPE at Θ = 2–3 BL as the

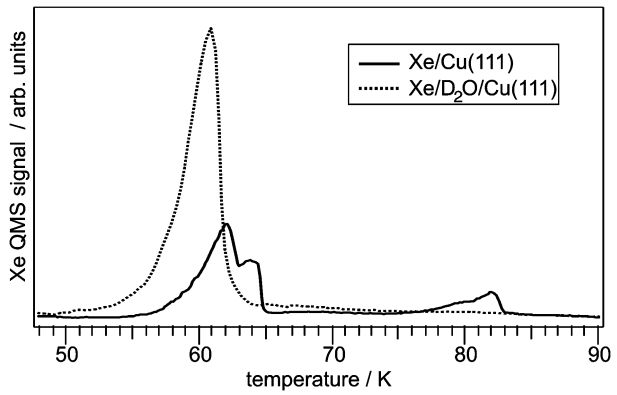

Fig. 2 Thermal desorption spectra of 4 ML xenon on Cu(111) (solid curve) and 6 ML xenon adsorbed on a D_2O layer on Cu(111) (dotted curve). The spectrum of Xe/Cu(111) shows three peaks at 62 K, 64 K and 82 K attributed to xenon atoms adsorbed in multilayers, second monolayer and first monolayer, respectively. In the case of xenon adsorbed on water, the TDS exhibits only one peak at around 60 K and is attributed to sublimation from a multilayer.

clusters coalesce.[34] Measurements by LT-STM revealed that the amorphous ice clusters have a height of 2–4 BL.[29,35]

First, we characterize Xe adsorption onto Cu(111) after exposure of the surface to a partial pressure of Xe at 30 K. The thermal desorption spectrum (TDS) of Xe/Cu(111) is depicted in Fig. 2 (solid curve) and exhibits three peaks. In good agreement with literature,[36] the peak at 82 K is associated with the desorption of the first monolayer of Xe. Features at 64 K and 62 K are attributed to the second monolayer and additional multilayers of Xe, respectively. The xenon coverage is determined from the TDS spectrum by normalization of the integrated intensity to the high temperature peak, *i.e.* to one complete monolayer of xenon adsorbed on the bare Cu(111) surface. In contrast to these observations we find no monolayer desorption peak for $Xe/D_2O/Cu(111)$ (Fig. 2, dotted curve). The Xe adsorbed on the closed ice layer desorbs exclusively *via* zero order desorption kinetics, suggesting that the interaction strength between the Xe atoms and the water ice is similar to the interatomic interaction within the Xe layer.

For 2PPE spectroscopy, femtosecond laser pulses at 800 nm are amplified in a commercial Ti:sapphire laser system (Coherent RegA 9050), which drives an optical parametrical amplifier (OPA). The signal output of the OPA serves as a time-delayed visible (VIS) probe. The signal's second harmonic serves as an ultraviolet (UV) pump. The pulse duration of pump and probe pulses is measured by their cross correlation on the sample. The full width at half maximum (FWHM) of the cross correlation of pump and probe is typically 60 fs. Fig. 1 shows the excitation mechanism. Absorption of the pump pulse excites an electron–hole pair in the metal. Since the photon energy is below the work function, the electron populates unoccupied bound electronic levels. The second, time-delayed probe pulse photoionizes the sample and the kinetic energy of the photoelectrons is then measured by an electron time-of-flight spectrometer (TOF) as a function of time delay. The energy E of intermediate states with respect to the Fermi level is then calculated by: $E - E_F = E_{kin} + \Phi - h\nu_{vis}$, where $\Phi = E_{vac} - E_F$ is the sample work function.

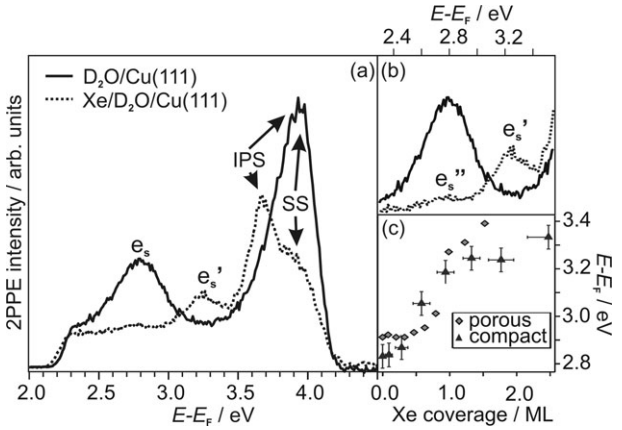

Fig. 3 (a) 2PPE spectra of compact amorphous ice clusters on Cu(111) before (solid curve) and after adsorption of 2 ML of Xe (dotted curve). The peak around 2.8 eV in the spectra (solid curve) originates from solvated electrons e_S, whereas the features at energies >3.3 eV arise from the Cu(111) surface state (SS) and first image potential state (IPS). After titration with xenon, e_S is shifted to higher energies by $\sim$400 meV (e'_S). (b) Expanded view of the 2PPE spectra around e_S. A small part of the solvated electron distribution e''_S is not affected by the adsorption of Xe. (c) Energy of the solvated electron's peak maximum as a function of Xe coverage for compact and porous ice cluster.

3. Results and discussion

3.1 Xe overlayer experiment

Fig. 3 shows 2PPE spectra of the Cu(111) substrate covered with compact amorphous ice clusters before (solid curve) and after (dotted curve) adsorption of 2 ML of Xe using photon energies of $h\nu_{vis} = 2.10$ eV and $h\nu_{UV} = 4.19$ eV. The 2PPE intensity is plotted as a function of intermediate state energy with respect to the Fermi level $E - E_F$.

Before adsorption of Xe on top of the ice clusters, the 2PPE spectrum of $D_2O/Cu(111)$ (black curve) is dominated by a peak around 3.9 eV, which is attributed to the surface state (SS) and the first image potential state (IPS) of bare Cu(111) remaining in between the ice clusters.[29,34] The overlap of these two features is due to the photon energies employed here. The second feature labelled e_S at $E - E_F = 2.8$ eV arises from solvated electrons, *i.e.* electrons which are localized in pre-existing traps below the edge of the ice conduction band and screened by the surrounding polar molecules.[20,37]

After adsorption of 2 ML of Xe the spectrum is clearly modified. On the bare Cu(111) surface the signal of the IPS is pinned to the local work function and exhibits a binding energy of 0.8 eV with respect to E_{vac}. Upon Xe exposure the work function of the formerly bare copper patches decreases, and additionally the binding energy of the IPS is decreased. In agreement with the literature[38] this leads to a shift of the IPS closer to the Fermi level and results in a more distinct separation of SS and IPS, as the occupied surface state of the Cu(111) surface does not change its energy. Furthermore, we find that the peak maximum of e_S shifts by more than 400 meV towards higher energies with respect to E_F, as depicted in Fig. 3c, as a function of Xe coverage. The energetic shift of e_S saturates after adsorption of one monolayer of xenon.

This significant change in the binding energy of the solvated electrons can be explained by a direct change of the dielectric environment of a surface-bound electron. As the rare gas atoms are inert, no chemical reaction takes place. Thus, the observed modification in the binding energy of the excess charge is caused by a perturbation of the potential of the excess electron. This electrostatic perturbation is attributed to the polarizability of the xenon atoms and might be accompanied by a modification of the spatial confinement of the e_S wave function. Thus, we conclude that in the case of ice clusters the solvated electrons bind at the ice–vacuum interface. A small fraction of the solvated electron distribution is not affected by the xenon atoms, as can be seen in Fig. 3b, where a small peak e''_S is observed at the same energetic position as before Xe adsorption. This feature may be attributed to solvated electrons, which are not perturbed by the rare gas atoms because they may reside in the bulk of the cluster. We also prepared clusters with a lower density of water molecules (porous amorphous clusters, see ref. 29) to investigate the influence of the cluster morphology on the binding site of the solvated electrons. We find that the spectral change upon Xe adsorption depicted in Fig. 3c (grey diamonds) is comparable with compact amorphous clusters (black symbols). Thus, the density of water molecules in the clusters and their morphology has no detectable influence regarding the probed binding site.

With increasing coverage at a nominal coverage of 2–3 BL,[34] the clusters laterally merge together forming a closed ice layer. Adsorption of further layers on top of the wetting ice layer does not change the binding energy and the stabilization rate of the solvated electrons, once the layer is formed.[34] Fig. 4 depicts the spectra of such a continuous amorphous ice layer (Θ = 4 BL) on Cu(111) before (solid curve) and after (dotted curve) adsorption of 2 ML of xenon. Here, the pump and probe energies are 3.76 eV and 1.87 eV, respectively. In the case of a closed ice layer, image potential and surface state of the substrate are absent as no bare copper patches are present. Both spectra are dominated by the peak of the solvated electrons around $E - E_F$ = 2.9 eV. Contrary to spectral changes upon titration with xenon presented in Fig. 3, the peak does not shift in the case of the wetting ice layer. The work function is increased by 90 meV after adsorption of 2 ML xenon as seen in the inset of Fig. 4, where the work function is depicted as a function of Xe coverage. For xenon adsorbed on a bare Cu(111) surface (Φ = 4.4 eV[38]) the work function is higher compared to D_2O/Cu(111) (Φ = 4.16 eV). Therefore Φ is expected to increase upon adsorption of Xe on top of D_2O/Cu(111). The fact that Xe adsorption has no influence on the binding energy of the solvated electrons shows that the solvated electrons are preferentially embedded within the bulk of closed ice multilayers. The polarizability of the xenon obviously does not affect the binding energy of the solvated electrons, which are already screened by the surrounding water molecules. Thus, screening by additional adsorbed Xe has, essentially, no further influence on the solvated electrons' binding energy.

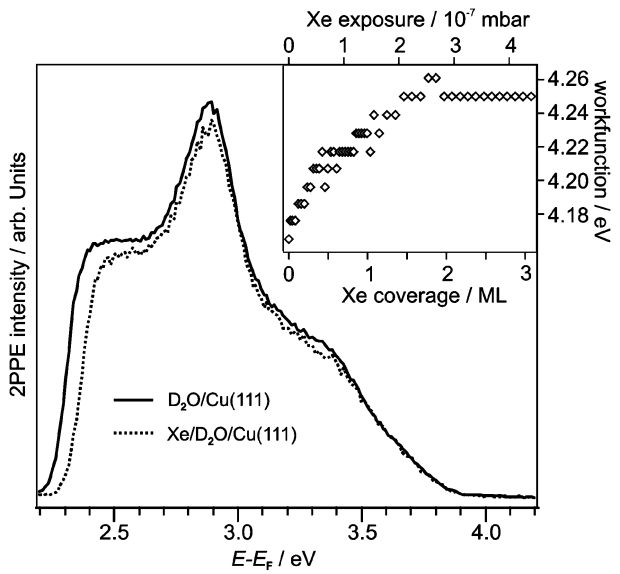

Fig. 4 2PPE spectra of 4 BL compact amorphous ice multilayer on Cu(111) before (solid curve) and after adsorption of 2 ML Xe (dotted curve). The peak of the solvated electron distribution does not shift upon Xe titration. Inset: shift of the work function upon xenon exposure. The work function increases by 90 meV at the saturation Xe coverage.

3.2 Time-resolved 2PPE spectroscopy

As we find that the solvated electron resides at the ice–vacuum interface for clusters and in the bulk of the film for wetting layers, we anticipate that a transition of the solvated electron's binding site occurs with the coalescence of the ice clusters to a smooth layer. As the cluster height does not change upon coalescence,[29] two scenarios appear reasonable. They are depicted in a schematic representation in the lower right panel of Fig. 5. (a) First, the solvated electron could reside at the maximum distance from the metal surface z_a at the top of the ice cluster and finds a more favourable site in the bulk of the smooth film only after coalescence. Thus the distance of the electron to the ice metal-interface would change upon

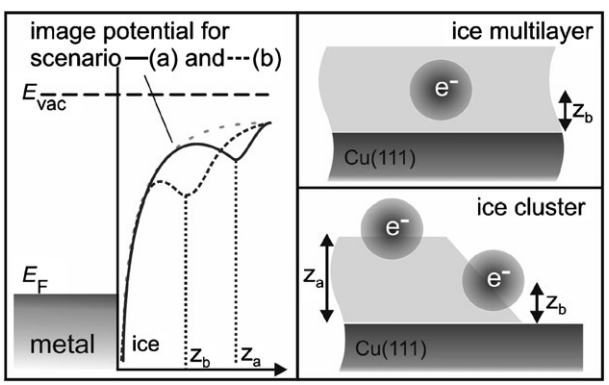

Fig. 5 Illustration of the modified image potential in the case of scenario (a)—solvation site on top of the cluster—and for scenario (b)—solvation site at the edge of the cluster (left panel). Right panels show the artists view of the bulk-bound solvated electrons in wetting ice layers and the two scenarios discussed for the surface-bound electrons in the case of ice clusters. For scenario (b) the distance between electron and metal surface is the same as for solvated electrons in the ice multilayer.

coalescence. In the second scenario (b) the solvated electron resides at the edges of the cluster and upon coalescence it automatically becomes a bulk state maintaining the distance to the ice–metal interface z_b. As none of the two scenarios can be excluded *a priori*, we employ further analysis to answer this question. The decay of the solvated electron on femtosecond timescales is sensitive to the electron's interaction with the metal substrate and the interaction is strongly z-dependent.[21] Therefore, we employed time-resolved 2PPE to investigate the decay process for the different structures. A conclusion on scenario (a) or (b) requires an empirical model calculation in addition: this model separates time-dependent population decay and energy gain through molecular rearrangement and has been developed earlier in ref. 39. In order to show which parameters of this model are sensitive to the environment of the solvated electrons, *i.e.* the amount and organisation of surrounding molecules, we primarily present time-dependent 2PPE data for porous and compact amorphous ice clusters. Data for ice multilayers have been published before in ref. 39. Subsequently, these parameters will be discussed with regard to the binding site determination.

The energetic shift of the solvated electron signal and the population decay are depicted in Fig. 6 for porous and compact amorphous ice clusters. Time-dependent 2PPE data on electron solvation dynamics are routinely analyzed in two different ways. (i) By following the solvated electron's peak maximum as a function of time-delay one can access the temporal evolution of the mean binding energy gain of the solvated electron. The interpretation of the observed peak shifts as a quantitative measure for electron stabilization has

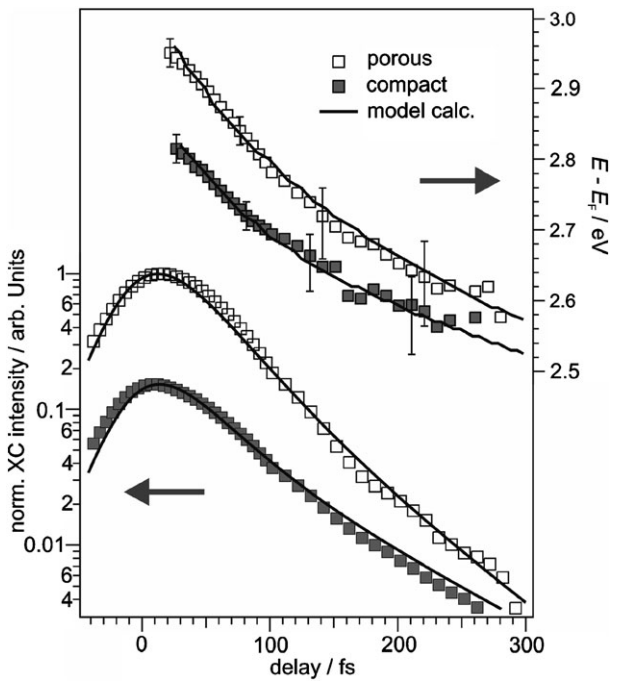

Fig. 6 Peak shift (top, right axis) and population decay (bottom, left axis) of solvated electrons as a function of time delay between pump and probe pulse for porous (open squares) and compact (solid squares) clusters. The electron dynamics are very well reproduced by the empirical model calculation (black curves) described in the text.

to be treated carefully as the transfer times are dependent on the energetic position of the electrons. An energy-dependent transfer time shifts the peak maximum of the solvated electron distribution towards lower energies.[39] The observed peak shift Σ_S is the sum of the stabilization σ_S and the additional peak shift δE resulting from energy-dependent electron transfer. The upper part of Fig. 6 shows the observed peak shift as a function of time-delay between pump and probe pulse (right axis) for compact and porous ice clusters. Linear fits to the time-dependent shifts of the peak maxima (not shown in the figure) yield a considerably faster shift of $\Sigma_S{}^p = -2.0(1)$ eV ps^{-1} for the porous clusters compared with the shift of $\Sigma_S{}^c = -1.3(1)$ eV ps^{-1} for the compact ones. The solvation process starts at higher energies with respect to E_F for the porous clusters. A distinct difference is also observed in the population dynamics. (ii) These dynamics can be accessed by integrating the 2PPE spectra in a certain energy window including the whole solvated electron energy distribution and plotting the cross correlation (XC) intensity as a function of time delay as shown in the lower part of Fig. 6 (left axis). Fitting a single exponential decay convoluted with the laser pulse envelope to the XC curves (not shown) gives a initial decay time of $\tau^c = 50(5)$ fs for the compact clusters compared to the porous clusters ($\tau^p = 36(5)$ fs). An explanation of the different dynamics of the solvated electrons on the basis of the above mentioned empirical model calculation is presented in the following, leading to a conclusion on the possible scenarios for surface binding sites.

As shown in ref. 39 the transfer dynamics of solvated electrons in D_2O can be separated into two regimes. At the beginning of the solvation process, the back transfer is mainly dominated by the electron's wave function overlap with unoccupied states of the metal and is therefore governed by the substrate's electronic properties. With ongoing solvation, a potential barrier develops between electron and metal and reduces the transfer probability. Now, the tunnelling through this barrier determines the electron transfer dynamics, which becomes increasingly independent of the metal substrate's properties. Furthermore, the decay time depends on the energetic position of the solvated electrons, which serves as a measure for their degree of solvation. We consider an energy-dependent decay time $\tau(E)$ to take into account both transfer regimes. For energies above the potential barrier maximum $E_{barrier}$, we assume a constant decay time τ_0, reflecting the influence of the surface electronic band structure of the metal substrate, and for $E \leq E_{barrier}$ an exponential energy dependence as expected for tunnelling processes:[39]

$$\tau(E) = \begin{cases} \tau_0 & \text{for } E_{barrier} < E \\ \tau_0 \exp[\gamma(E_{barrier} - E)] & \text{for } E_{barrier} \geq E \end{cases}$$

The exponential factor γ is attributed to the screening efficiency, describing the dynamic response of the water molecules to the excess charge. The larger this value is, the more the decay time is enhanced with increasing binding energy. The solvated electron population changes as a function of time

following the equation:[39]

$$\frac{\partial N(t,E)}{\partial t} = \underbrace{-\left(\sigma_S + \frac{1}{\tau(E)}\right)N(t,E)}_{\text{i}} + \underbrace{\left(\sigma_S - \frac{1}{\tau(E+\delta E)}\right)N(t,E+\delta E)}_{\text{ii}}$$

Here $N(t,E)$ is the population at the energy E and at a given time t after photoinjection. It is (i) decreased due to the back transfer to the metal with a rate $\tau^{-1}(E)$ and a successive stabilization to lower energies $E - \delta E$ with a constant rate σ_S. Simultaneously the number of electrons is (ii) increased due to electrons stabilizing from higher energies $E + \delta E$ and having a back transfer rate $\tau^{-1}(E + \delta E)$.

As seen in Fig. 6, the time-dependent binding energy and population decay is very well reproduced by the empirical model described above for both types of clusters (black curves). Table 1 presents the parameters resulting from the model calculation for porous and compact clusters. For comparison, also the model parameters for wetting multilayers are given (taken from ref. 39). The initial decay τ_0, and the energy difference $\Delta E = E_{barrier} - E_0$ between the barrier maximum and the maximum of the solvated electron distribution at $t = 0$ are identical for porous and compact ice clusters. τ_0 is a direct measure of the coupling degree of the electron with the metal substrate right after photoexcitation, and ΔE describes the influence of the initial solvent induced screening before enhanced screening due to further solvation occurs. This shows that the initial screening is similar for both types of clusters. Furthermore, the stabilization rate σ_S is identical in both cases. The only difference obtained in the cluster parameters is the screening efficiency γ, as this value is almost doubled for compact clusters compared to porous clusters. This result shows that the differences in both population decay and peak shift for the two types of clusters (Fig. 6) are solely due to a more efficient screening of the excess charge for compact clusters. We can conclude that a higher density of surrounding water molecules, *i.e.* a higher dipole density, results in a slower back transfer of the solvated electrons to the metal. More water dipoles between the electron and the metal surface are involved in the screening of the excess charge, resulting in longer lifetimes. If the electron was localized on top of the clusters, this would mean that this density effect dominates over the influence of the enhanced electron–metal distance in the case of porous ice, as they are up to 1 BL higher than compact clusters.[29]

Table 1 Parameters resulting from the empirical model for the 4 BL wetting D_2O multilayer (taken from ref. 39), for porous and compact D_2O clusters. The screening efficiency γ is normalized to the value of the ice multilayer

	σ_S/eV ps^{-1}	τ_0/fs	ΔE/meV	γ (γ^{ML})
Porous	0.22	25	−20	0.45
Compact	0.22	25	−20	0.8
Multilayer	0.22	67	+30	1

Comparison of these parameters to the water multilayer reveals a better initial screening for the D_2O layer. The initial decay time τ_0 is almost three times larger, representing a weaker initial electronic coupling to the metal for multilayers. In addition, the influence of the solvent, expressed by ΔE, is larger. It appears that the higher number of surrounding molecules in the wetting layer leads to a stronger initial screening of the excess charge. This is reasonable, since the solvated electrons reside in the bulk of ice layers. Also the dynamic response of the D_2O molecules, described by the exponential factor γ, is larger for the multilayer compared to both cluster types. Remarkably, the stabilization rate σ_S is the same for all investigated water structures on Cu(111) surfaces. This means that the reorganization of the water molecules results in a similar stabilization energy of the solvated electrons independently of the different structures adsorbed. As a possible explanation we consider a competition of two effects. As surface molecules are less coordinated than bulk molecules one expects them to be more mobile resulting in a more efficient response of the solvent. On the other hand, in the solvation process of bulk-bound electrons, more water molecules are involved, leading to a better energetic stabilization. It is well possible that both effects cancel each other.

3.3 Discussion

The analysis of the time-dependent 2PPE data using the presented empirical model calculation and the results of the titration experiment with xenon enable us to make a decision in favour of one of the proposed scenarios for surface solvation in case of ice clusters depicted in Fig. 5. As shown in section 3.1, the excess electrons are bound at the ice/vacuum interface of the D_2O clusters. As we found from the comparison of compact and porous clusters, the higher number of water molecules in between the localized electron and the metal surface results in a more efficient screening, *i.e.* a higher γ value. In case of the proposed scenario (a) – the solvated electron resides at the top of the cluster – the distance of the electron to the metal-interface z_a (Fig. 5) would be larger compared to a 3 BL thick multilayer, where the electron resides in the bulk. Therefore one would expect the screening to be less efficient for the multilayer than for the compact clusters. Furthermore, due to the larger distance one would expect a longer initial decay time τ_0 of the solvated electrons in the ice clusters. Neither of these consequences is supported by our findings. Hence we exclude scenario (a). In scenario (b) the electrons bind on the edges of the flat lying ice clusters. In this case the distance of the electrons to the metal substrate would be comparable to that of the bulk-bound species in the ice multilayer z_b (see Fig. 5). This is reasonable if we take into account the image potential in front of the metal surface. The left panel of Fig. 5 depicts schematically the modified image potentials (IP) for both proposed scenarios. The rearrangement of the water molecules in the vicinity of the solvated electron modifies the IP producing local minima. Solvation sites closer to the metal surface are favoured as more energy is gained with respect to the vacuum level. However, as the average coordination number is smaller at the edges compared to a bulk site, less efficient screening of the solvated electrons

on the ice clusters is expected, which is consistent with the experimental observation (Table 1). In addition, the Xe titration of the ice clusters revealed that a small fraction of the solvated electron feature in the 2PPE spectrum is not affected by the rare gas layer (e''_S in Fig. 3b), attributed to bulk-bound species, whereas no surface-bound electrons are observed in wetting ice layers. This disappearance of the surface-bound species upon coalescence can be explained by solvated electrons residing at the edge of the clusters, electrons on top of the clusters would not be affected. The transition of the binding site can be viewed as a consequence of the coalescence of the clusters with increasing coverage. In this sense, the more efficient screening of the excess electrons in ice layers can be explained as follows. Inside the layer, the excess charge is surrounded by water molecules. Fewer molecules are involved in the screening of the edge-bound electrons, which is supported by a stronger initial coupling to the metal and a lower screening efficiency reported in Table 1. Hence, binding sites at the edge of the porous and compact D_2O clusters appear to be the most probable scenario for electron solvation at ice cluster–vacuum interfaces.

4. Conclusion

In this work we have investigated the electron's solvation site in amorphous D_2O ice clusters and wetting multilayers by means of 2PPE spectroscopy. By titration of the binding sites with xenon overlayers we find solvated electrons which are embedded in the bulk of a closed ice film. A strong shift of the electron's spectral feature upon xenon adsorption by $\sim$400 meV for ice clusters reveals the solvation site of these electrons to be located at the ice–vacuum interface. Since the back transfer of the electrons to the metal surface is sensitive to the coupling strength to substrate states and thus to the distance of the binding site to the substrate, a more detailed determination of the binding site is possible by performing an analysis of relaxation dynamics in the time domain. By a comparison of porous and compact amorphous ice clusters the environment of the solvated electrons is analysed in the respective structures. Subsequently, we demonstrate that an electron solvation at the edges of the clusters is the most probable scenario and conclude that the transition between bulk- and surface-bound solvated electrons is mediated by the coalescence of the clusters forming a closed ice film.

Acknowledgements

We acknowledge funding by the Deutsche Forschungsgemeinschaft through Sfb 450 and by the German-Israeli Foundation.

References

1. E. J. Hart and J. W. Boag, *J. Am. Chem. Soc.*, 1962, **84**, 4090.
2. R. Santucci, T. Ferri, L. Morpurgo, I. Savini and L. Avigliano, *Biochem. J.*, 1998, **332**, 611.
3. Q. B. Lu and T. E. Madey, *J. Chem. Phys.*, 1999, **111**, 2861.
4. Q. B. Lu and L. Sanche, *Phys. Rev. B*, 2001, **63**, 153403.
5. J. V. Coe, G. H. Lee, J. G. Eaton, S. T. Arnold, H. W. Sarkas, K. H. Bowen, C. Ludewigt, H. Haberland and D. R. Worsnop, *J. Chem. Phys.*, 1990, **92**, 3980.
6. P. Ayotte and M. A. Johnson, *J. Chem. Phys.*, 1997, **106**, 811.
7. N. I. Hammer, J.-W. Shin, J. M. Headrick, E. G. Diken, J. R. Roscioli, G. H. Weddle and M. A. Johnson, *Science*, 2004, **306**, 675.
8. A. E. Bragg, J. R. R. Verlet, A. Kammrath, O. Cheshnovsky and D. M. Neumark, *Science*, 2004, **306**, 669.
9. D. H. Paik, I.-R. Lee, D. S. Yang, J. S. Baskin and A. H. Zewail, *Science*, 2004, **306**, 672.
10. J. V. Coe, *Int. Rev. Phys. Chem.*, 2001, **20**, 22.
11. R. N. Barnett, U. Landman, C. L. Cleveland and J. Jortner, *J. Chem. Phys.*, 1998, **88**, 4429.
12. J. R. R. Verlet, A. E. Bragg, A. Kammrath, O. Cheshnovsky and D. M. Neumark, *Science*, 2005, **307**, 93.
13. R. N. Barnett, U. Landman and A. Nitzan, *Phys. Rev. Lett.*, 1989, **62**, 106.
14. L. Turi, W.-S. Sheu and P. J. Rossky, *Science*, 2005, **309**, 914.
15. F. Zappa, S. Denifl, I. Mähr, A. Bacher, O. Echt, T. D. Märk and P. Scheier, *J. Am. Chem. Soc.*, 2008, **130**, 5573.
16. C. M. Wong, J. D. McNeill, K. J. Gaffney, N.-H. Ge, A. D. Miller, S. H. Liu and C. B. Harris, *J. Phys. Chem. B*, 1999, **103**, 282.
17. J. Zhao, B. Li, K. Onda, M. Feng and H. Petek, *Chem. Rev.*, 2006, **106**, 4402.
18. A. D. Miller, I. Bezel, K. J. Gaffney, S. Garrett-Roe, S. H. Liu, P. Szymanski and C. B. Harris, *Science*, 2002, **297**, 1163.
19. B. Li, J. Zhao, K. Onda, K. D. Jordan, J. Yang and H. Petek, *Science*, 2006, **311**, 1436.
20. C. Gahl, U. Bovensiepen, C. Frischkorn and M. Wolf, *Phys. Rev. Lett.*, 2002, **89**, 107402.
21. J. Stähler, M. Meyer, D. O. Kusmierek, U. Bovensiepen and M. Wolf, *J. Am. Chem. Soc.*, 2008, **130**, 27.
22. K. Onda, B. Li, J. Zhao, K. D. Jordan, J. Yang and H. Petek, *Science*, 2005, **308**, 1154.
23. S. Ryu, J. Chang, H. Kwon and S. K. Kim, *J. Am. Chem. Soc.*, 2006, **128**, 3500.
24. M. Bertin, M. Meyer, J. Stähler, C. Gahl, M. Wolf and U. Bovensiepen, *Faraday Discuss.*, in press.
25. D. Nordlund, H. Ogasawara, H. Bluhm, O. Takahashi, M. Odelius, M. Nagasono, L. G. M. Pettersson and A. Nilsson, *Phys. Rev. Lett.*, 2007, **99**, 217406.
26. M. Wolf, E. Knoesel and T. Hertel, *Phys. Rev. B*, 1996, **54**, R5295.
27. A. Hotzel, M. Wolf and J. P. Gauyacq, *J. Phys. Chem. B*, 2000, **104**, 8438.
28. J. D. McNeill, R. L. Lingle, Jr, N.-H. Ge, C. M. Wong, R. E. Jordan and C. B. Harris, *Phys. Rev. Lett.*, 1997, **79**, 4645.
29. J. Stähler, M. Mehlhorn, U. Bovensiepen, M. Meyer, D. O. Kusmierek, K. Morgenstern and M. Wolf, *Phys. Rev. Lett.*, 2007, **98**, 206105.
30. U. Bovensiepen, *Prog. Surf. Sci.*, 2005, **78**, 87.
31. G. A. Kimmel, N. G. Petrik, Z. Dohnálek and B. D. Kay, *J. Chem. Phys.*, 2006, **125**, 044713.
32. E. D. Sloan and C. A. Koh, *Clathrate Hydrates of Natural Gases*, CRC Press, London, 3rd edn, Chemical Industries, 2007, vol. 119.
33. E. Knoesel, A. Hotzel and M. Wolf, *Phys. Rev. B*, 1998, **57**, 12812.
34. C. Gahl, U. Bovensiepen, C. Frischkorn, K. Morgenstern, K.-H. Rieder and M. Wolf, *Surf. Sci.*, 2003, **108**, 532.
35. M. Mehlhorn and K. Morgenstern, *Phys. Rev. Lett.*, 2007, **99**, 246101.
36. W. Berthold, F. Rebentrost, P. Feulner and U. Höfer, *Appl. Phys. A*, 2004, **78**, 131.
37. U. Bovensiepen, C. Gahl and M. Wolf, *J. Phys. Chem. B*, 2003, **107**, 8706.
38. M. Wolf, E. Knoesel and T. Hertel, *Phys. Rev. B*, 1996, **54**, 5295.
39. J. Stähler, C. Gahl, U. Bovensiepen and M. Wolf, *J. Phys. Chem. B*, 2006, **110**, 9637.

